JACS
JOURNAL OF THE AMERICAN CHEMICAL SOCIETY

Article

pubs.acs.org/JACS

In Situ Growth of $Co_{0.85}Se$ and $Ni_{0.85}Se$ on Conductive Substrates as High-Performance Counter Electrodes for Dye-Sensitized Solar Cells

Feng Gong, Hong Wang, Xin Xu, Gang Zhou, and Zhong-Sheng Wang*

Department of Chemistry, Laboratory of Advanced Materials, Fudan University, 2205 Songhu Road, Shanghai 200438, P.R. China

Supporting Information

ABSTRACT: We present herein a facile one-step low-temperature hydrothermal approach for in situ growth of metal selenides ($Co_{0.85}Se$ and $Ni_{0.85}Se$) on conductive glass substrates. The as-prepared metal selenides on conductive substrates can be used directly as transparent counter electrodes for dye-sensitized solar cells (DSSCs) without any post-treatments. It is found that graphene-like $Co_{0.85}Se$ exhibits higher electrocatalytic activity than Pt for the reduction of triiodide. As a consequence, the DSSC with $Co_{0.85}Se$ generates higher short-circuit photocurrent and power conversion efficiency (9.40%) than that with Pt.

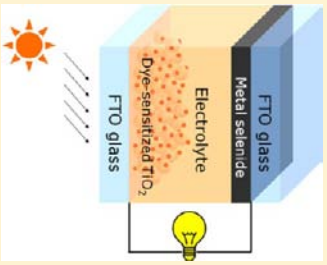

INTRODUCTION

As one of the most promising alternatives for traditional silicon solar cells, dye-sensitized solar cells (DSSCs) have attracted tremendous scientific and industrial attention in the past two decades, owing to their low cost, environmental friendliness, simple production processes, and high efficiency.[1] A typical DSSC has a sandwich structure with a photoanode comprising TiO_2 nanocrystals sensitized by dye molecules, an electrolyte containing the iodide/triiodide (I^-/I_3^-) redox couple, and a counter electrode (CE) catalyzing the reduction of I_3^- to I^-. Usually, platinum is the preferred material for catalyzing the reduction of I_3^- due to its superior conductivity, electrocatalytic activity, and stability. However, as a noble metal, low abundance ratio and high cost prevent Pt from being used for large-scale manufacturing of DSSCs, which has stimulated great efforts to exploit substitutes for Pt in order to reduce the overall cost and simultaneously keep the performance of DSSC.[2]

Carbonaceous materials[3] and conductive polymers[4] have been proposed as CEs to replace Pt in DSSCs, but their stabilities and catalytic activities are not satisfactory. To improve the catalytic activity, a self-assembled graphene/Pt monolayer film with an extremely low loading amount of Pt was developed, and good performance was achieved using this ultrathin film as CE for a DSSC.[5] Recently, some inorganic compounds have also been introduced into DSSCs as electrocatalysts, such as sulfides,[2,6] nitrides,[7] and carbides,[8] which show good catalytic activity as CE materials. Lately, the need for low-cost, scalable, and solution-processable photovoltaic materials gives great impetus to the research on the synthesis of semiconductor nanocrystals.[9] As an important class of chalcogenides, semiconducting selenides have drawn enormous attention due to their distinctive electronic properties, interesting chemical behaviors, and wide variety of potential applications.[10] To the best of our knowledge, no research on in situ growth of binary metal selenides on conductive substrates for use in DSSCs as electrocatalysts has been reported so far.

Herein, we propose a facile one-step strategy to synthesize cobalt selenide ($Co_{0.85}Se$) and nickel selenide ($Ni_{0.85}Se$) in situ on conductive glass substrates and use them directly as CEs to assemble DSSCs without any post-treatments such as heating or coating with other ancillary materials. When applied as the CE in DSSCs, graphene-like $Co_{0.85}Se$ achieved a power conversion efficiency (PCE) of 9.40% versus 8.64% for Pt under the same conditions. To the best of our knowledge, this is the highest PCE for I^-/I_3^- redox couple based DSSCs with Pt-free cathodes under AM1.5G simulated solar light (100 mW cm^{-2}).

EXPERIMENTAL SECTION

Preparation of Selenide and Pt Electrodes. Se powder (0.024 mmol, 99.999%, Aladding) and $CoCl_2 \cdot 6H_2O$ (0.02 mmol, 99.9%, Alfa Aesar) or $NiCl_2 \cdot 6H_2O$ (0.02 mmol, 99.9%, Alfa Aesar) dissolved in 5.5 mL of deionized water were added to a 10 mL Teflon-lined autoclave in sequence, and then 1.5 mL of $N_2H_4 \cdot H_2O$ (85 wt %, Sinopharm) was added with vigorous stirring for 10 min. Transparent conductive glass (F-doped SnO_2, FTO, 15 Ω/square, transmittance of 80%) was received from Nippon Sheet Glass Co., Japan. A piece of cleaned FTO substrate was put in the autoclave and placed at an angle against the wall of the Teflon liner with the conducting side facing down. The autoclave was sealed and maintained at 120 °C for 12 h. To prepare Pt CEs, 50 μL of H_2PtCl_6 in ethanol was drop-cast on 1.5 × 1.5 cm^2 FTO glass substrates, followed by heat treatment at 380 °C for 30 min.

Fabrication of DSSCs. TiO_2 films (15 μm thick) containing transparent (11 μm) and scattering (4 μm) layers were prepared according to a previous report.[11] TiO_2 films were soaked overnight in *cis*-di(isothiocyanato)-bis-(2,2′-bipyridyl-4,4′-dicarboxylato)ruthenium-(II) bis-tetrabutylammonium (so-called N719, used as received from Solaronix SA) solution (0.3 mM in a mixed solvent of acetonitrile and *tert*-butanol in a volume ratio of 1:1). The dye-sensitized TiO_2 photoanode and the CE were separated by a hot-melt Surlyn film

Received: April 5, 2012
Published: June 1, 2012

   dx.doi.org/10.1021/ja303034w | J. Am. Chem. Soc. 2012, 134, 10953−10958

(30 μm thick) and sealed through hot-pressing. The redox electrolyte (0.1 M LiI, 0.05 M I_2, 0.6 M 1,2-dimethyl-3-*n*-propylimidazolium iodide, and 0.5 M 4-*tert*-butylpyridine in anhydrous acetonitrile) was injected into the interspace between the photoanode and CE. Finally, the holes on the back of the CE were sealed with a Surlyn film covered with a thin glass slide under heat.

Characterizations. X-ray diffraction (XRD) profiles of the obtained selenides were recorded on an X-ray powder diffractometer (D8 Advance, Bruker) with Cu Kα radiation (λ = 0.154 nm). The optical transmittance spectra of as-prepared selenide cathodes were measured on a Shimadzu UV-2550 UV−vis spectrometer. The morphology and microstructure of the selenide CEs were examined by field emission scanning electron microscopy (FESEM, S-4800, Hitachi) and high-resolution transmission electron microscopy (HRTEM, JEM-2100F, JEOL). The composition and loading amount of selenides on substrates were detected by inductively coupled plasma−atomic emission spectra (ICP−AES, Thermo Electron Corp. Adv. ER/S). Before the ICP measurements, the selenide CEs were immersed in concentrated nitric acid with agitation for 12 h to dissolve the compounds from the substrate. The specific surface area was measured with a Micromeritics ASAP2020 nitrogen adsorption−desorption apparatus. Cyclic voltammetry (CV) was carried out in a three-electrode system containing an anhydrous acetonitrile solution of 0.1 M $LiClO_4$, 10 mM LiI, and 1 mM I_2 at a scan rate of 50 mV s^{-1}, using a Pt wire as the CE, an Ag/Ag^+ electrode as the reference electrode, and the as-prepared CE as the working electrode. For electrochemical impedance spectroscopy (EIS) and polarization measurements, the symmetrical dummy cells were assembled with two identical CEs filled with the same electrolyte as used in the DSSCs. The active apparent area of the dummy cell was 0.36 cm^2. In EIS tests, the samples were scanned from 0.1 Hz to 500 kHz at 0 V bias and ac amplitude of 10 mV. The polarization measurements were performed at a scan rate of 50 mV s^{-1}. All the electrochemical characterizations were performed on an electrochemical workstation (ZAHNER ZENNIUM CIMPS-1, Germany). The photocurrent density−voltage curves of DSSCs were recorded on a Keithley 2400 source meter under the illumination of AM1.5G simulated solar light coming from an AAA solar simulator (Newport-94043A) equipped with a Xe lamp (450 W) and an AM1.5G filter. The light intensity was calibrated using a reference Si solar cell (Oriel-91150). A black mask with an aperture area of 0.2304 cm^2 was applied on the surface of DSSCs to avoid stray light completely.

RESULTS AND DISCUSSION

Characterizations of the Selenides and As-Prepared CEs. The metal selenides could grow in situ on well-cleaned FTO glass substrates from a precursory mixture solution (see Experimental Section) in a Teflon-lined autoclave through a hydrothermal reaction.[10] The best metal selenide CEs in terms of solar cell performance were obtained at reaction temperature of 120 °C for 12 h. The XRD patterns of the selenide products are shown in Figure 1. The peak positions can be well indexed to $Co_{0.85}Se$ (JCPDS No. 52-1008) and $Ni_{0.85}Se$ (JCPDS No. 18-0888), as shown in Figure 1. After the hydrothermal procedure, FTO glass turned shallow black but still kept high optical transparency (>85% in the visible region), as shown in Figure 2. The transparency of the CE provides added value for many practical applications such as windows, roof panels, or various decorative installations, although it is not critical for the function of DSSCs.[3d] In addition, transparent CE is useful to construct tandem solar cells.

The compositions of the selenides and loading amounts on FTO were determined by ICP−AES. The results show that the atomic ratios are 0.845:1.000 for Co:Se and 0.841:1.000 for Ni:Se, which are close to the stoichiometry of $Co_{0.85}Se$ and $Ni_{0.85}Se$, respectively. The loading amounts of $Co_{0.85}Se$, $Ni_{0.85}Se$, and Pt on the substrate were determined to be 8.7, 5.3, and 23.0 μg cm^{-2}, respectively. Specific surface areas of 11.8, 16.7, and 5.8 m^2 g^{-1} were measured for $Co_{0.85}Se$, $Ni_{0.85}Se$, and Pt, respectively.

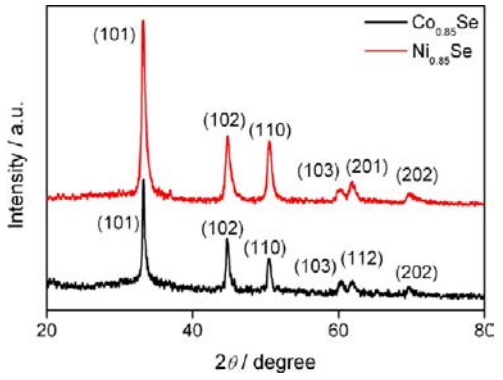

Figure 1. XRD patterns of the selenide products.

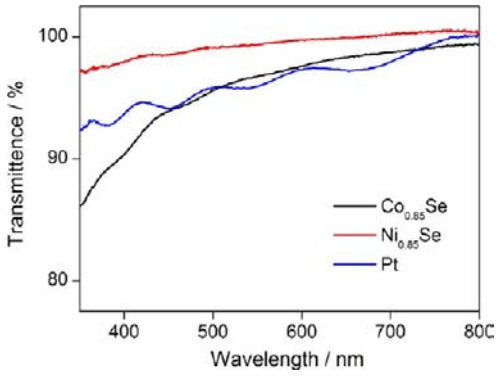

Figure 2. Optical transmittance spectra of $Co_{0.85}Se$, $Ni_{0.85}Se$, and Pt CEs.

Figure 3 shows the FESEM images of $Co_{0.85}Se$ and $Ni_{0.85}Se$ grown in situ on FTO substrates with different magnifications.

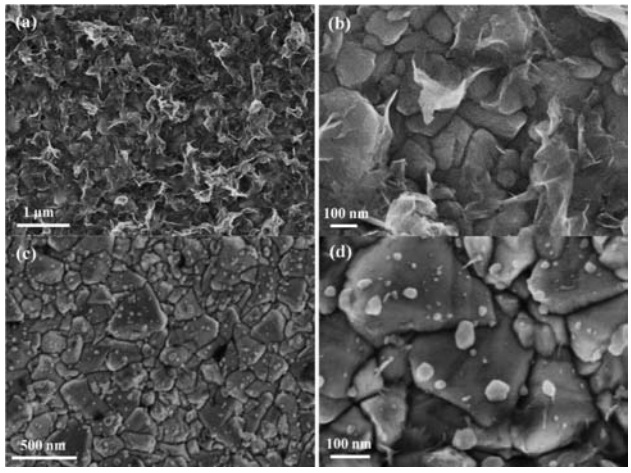

Figure 3. FESEM images of $Co_{0.85}Se$ (a,b) and $Ni_{0.85}Se$ (c,d) grown in situ on FTO glass at different magnifications.

$Co_{0.85}Se$ and $Ni_{0.85}Se$ with different morphologies were successfully grown on FTO substrates, but the FTO surface was not covered fully by the selenides, as revealed by the clear observation of scalelike FTO layer. The relatively low surface coverage of $Co_{0.85}Se$ and $Ni_{0.85}Se$ is responsible for their high transparency. Moreover, $Co_{0.85}Se$ has a higher surface coverage

dx.doi.org/10.1021/ja303034w | J. Am. Chem. Soc. 2012, 134, 10953−10958

and loading than $Ni_{0.85}Se$, which supports that the former has a lower transparency than the latter (Figure 2). The as-prepared $Co_{0.85}Se$ exhibits a foliate structure (Figure 3a,b) just like graphene, which is similar to a recent report.[12] By contrast, spherical nanoparticles are observed for $Ni_{0.85}Se$ grown on FTO (Figure 3c,d). Energy dispersive spectroscopy (EDS, Figure S1 in Supporting Information) analysis demonstrates the presence of Co and Se for $Co_{0.85}Se$ and Ni and Se for $Ni_{0.85}Se$ with atomic ratios close to their stoichiometry.

The morphologies of the formed metal selenides are further characterized through HRTEM, as depicted in Figure 4.

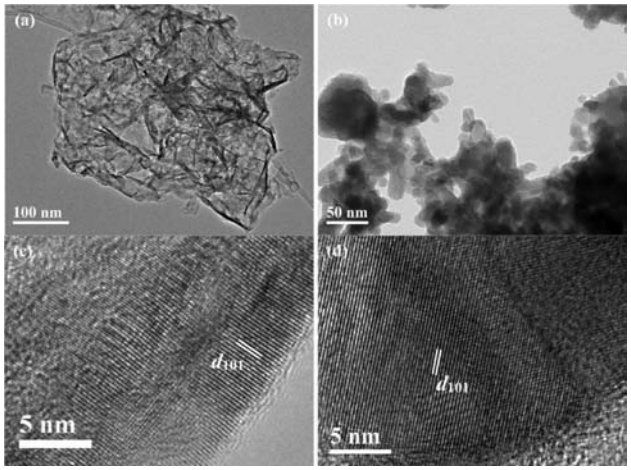

Figure 4. HRTEM images of as-synthesized $Co_{0.85}Se$ (a,c) and $Ni_{0.85}Se$ (b,d).

$Co_{0.85}Se$ presents a graphene-like structure, possessing large surface area. On the other hand, $Ni_{0.85}Se$ obtained by hydrothermal reaction mainly exhibits particulate shape with aggregation. The clear observation of lattice fringes (Figures 4c,d) for the metal selenides indicates that the formed $Co_{0.85}Se$ and $Ni_{0.85}Se$ have good crystallinity. The interplanar spacings of d_{101} derived from the lattice fringes are 2.7 ± 0.1 Å for both $Co_{0.85}Se$ and $Ni_{0.85}Se$, which are in good coincidence with the theoretical values (d_{101} = 2.69 Å for $Co_{0.85}Se$ and d_{101} = 2.70 Å for $Ni_{0.85}Se$).

Photovoltaic Performance. Figure 5 compares the photovoltaic performance of N719-sensitized solar cells assembled with various cathodes, and the corresponding photovoltaic performance parameters are summarized in Table 1. The DSSC with $Co_{0.85}Se$-loaded CE yielded a remarkable PCE of 9.40% (short-circuit photocurrent density (J_{sc}) = 16.98 mA cm^{-2}, open-circuit photovoltage (V_{oc}) = 738 mV, fill factor (FF) = 0.75), while the DSSC with $Ni_{0.85}Se$ CE produced a PCE of 8.32% (J_{sc} = 15.63 mA cm^{-2}, V_{oc} = 739 mV, FF = 0.72). For reference, the Pt-coated CE-based DSSC was also measured under the same condition, giving a PCE of 8.64% (J_{sc} = 16.03 mA cm^{-2}, V_{oc} = 738 mV, FF = 0.73). J_{sc} increased in the order of $Ni_{0.85}Se$ < Pt < $Co_{0.85}Se$, and PCE increased in the same order. Evidently, $Co_{0.85}Se$ performs better than Pt as the CE in DSSCs. The obtained efficiency is impressive for a Pt-free electrochemical catalyst. To the best of our knowledge, this is the highest PCE for I^-/I_3^- redox couple based DSSCs with Pt-free cathodes under AM1.5G simulated solar light (100 mW cm^{-2}). As the CEs are transparent, PCE can be further improved by putting a reflective mirror on the back of the CE.

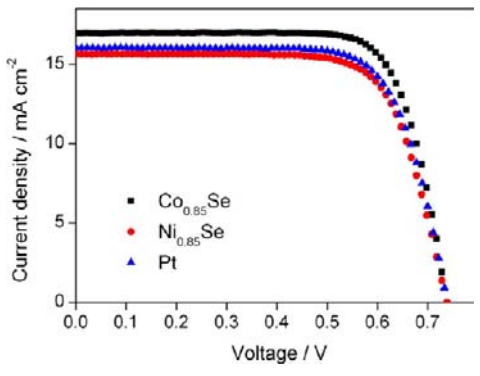

Figure 5. Photocurrent density−voltage characteristics of DSSCs with different CEs, measured at AM1.5G illumination (100 mW cm^{-2}).

Electrochemical Behaviors. To interpret the J_{sc} difference, the electrocatalytic activity of various CEs, which has a positive correlation with the photocurrent generation, was evaluated by CV. Figure 6 gives the CV curves of iodide/triiodide redox species using $Co_{0.85}Se$, $Ni_{0.85}Se$, and Pt electrodes, respectively. For all the three electrodes, two pairs of oxidation and reduction peaks (Ox-1/Red-1, Ox-2/Red-2) are well resolved, as labeled in Figure 6. The left and right pairs are described by eqs 1 and 2, respectively.

$$I_3^- + 2e^- \leftrightarrow 3I^- \quad (1)$$

$$3I_2 + 2e^- \leftrightarrow 2I_3^- \quad (2)$$

Since the CE of a DSSC is responsible for catalyzing the reduction of I_3^- to I^-, the characteristics of peaks Ox-1 and Red-1 are at the focus of our analysis. The peak currents and the peak-to-peak separation (E_{pp}), which is negatively correlated with the standard electrochemical rate constant of a redox reaction, are two important parameters for comparing catalytic activities of different CEs.[13] The higher peak current densities and lower E_{pp} value (Table 1) reveal that $Co_{0.85}Se$ is a remarkable electrochemical catalyst for the reduction of I_3^-, even better than the Pt electrode. Judged from the lower peak currents and larger E_{pp}, $Ni_{0.85}Se$ is inferior to Pt and $Co_{0.85}Se$, but still exhibits good electrocatalytic activity.

To further elucidate the catalytic activities of different CEs on the reduction of triiodide, EIS experiments were carried out using symmetric cells fabricated with two identical electrodes (CE/electrolyte/CE). The Nyquist plots (Figure 7) for symmetric cells with different CEs illustrate impedance characteristics, in which two semicircles are observed in the higher (left) and lower (right) frequency regions. According to the Randles-type circuit (inset of Figure 7), the high-frequency intercept on the real axis represents the series resistance (R_s). The left arc arises from the charge-transfer resistance (R_{ct}) at the CE/electrolyte interface, which changes inversely with the catalytic activity of different CEs on the reduction of triiodide, and the corresponding constant phase element (CPE), while the right one stems from the Nernst diffusion impedance (Z_N) of the I^-/I_3^- redox couple in the electrolyte.[3d] These parameters were determined by fitting the impedance spectra using the Z-view software, and good agreement between the measured and the fitted data was achieved in all cases. The resistance and impedance shown in Table 1 were calculated using the total surface area of catalysts on the electrode of the dummy cell. The total surface area obtained by the production

dx.doi.org/10.1021/ja303034w | J. Am. Chem. Soc. 2012, 134, 10953−10958

Table 1. Photovoltaic and Electrochemical Performance Parameters for Different CEs

CE	V_{oc}/mV	J_{sc}/mA cm^{-2}	FF	PCE/%	R_s/Ω cm^2	R_{ct}/Ω cm^2	Z_N/Ω cm^2	E_{pp}/mV
$Co_{0.85}Se$	738	16.98	0.75	9.40	2.1	0.6	0.5	342
$Ni_{0.85}Se$	739	15.63	0.72	8.32	1.8	1.8	1.4	581
Pt	738	16.03	0.73	8.64	2.6	1.1	0.9	414

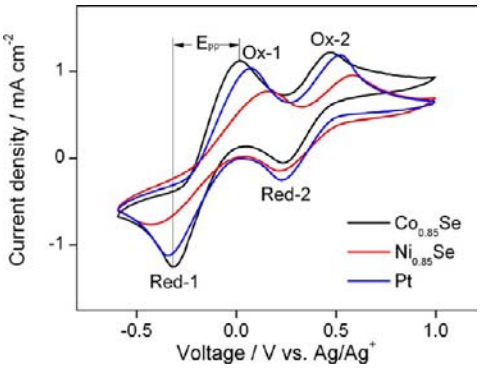

Figure 6. CV curves of iodide/triiodide redox species for $Co_{0.85}Se$, $Ni_{0.85}Se$, and Pt electrodes, respectively.

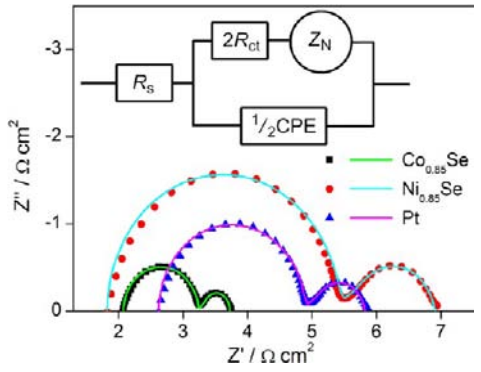

Figure 7. Nyquist plots for symmetric cells fabricated with $Co_{0.85}Se$, $Ni_{0.85}Se$, and Pt CEs. The lines express fit results for corresponding EIS data, and the inset gives the equivalent circuit.

of specific surface area, loading amount, and the active apparent area (0.36 cm^2) of the electrode is 0.37, 0.32, and 0.48 cm^2 for $Co_{0.85}Se$, $Ni_{0.85}Se$, and Pt, respectively.

As the three CEs have nearly the same absolute R_s, the effect of various CEs caused by R_s on photovoltaic performance can be omitted. The R_{ct} increases in the order of $Co_{0.85}Se$ (0.6 Ω cm^2) < Pt (1.1 Ω cm^2) < $Ni_{0.85}Se$ (1.8 Ω cm^2), indicating an inverse order of catalytic activity. The smallest R_{ct} for $Co_{0.85}Se$ implies that it has eximious catalytic activity on the reduction of triiodide and supersedes the expensive Pt as the CE in DSSCs. The conclusions for the catalytic activity derived from the EIS and CV data are consistent.

As the electrocatalytic activity may depend on the morphology, we prepared particulate $Co_{0.85}Se$ in a mixed solvent of acetonitrile and water (volume ratio of 3.5:2.0), which was characterized with HRTEM (Figure S2a,b), FESEM (Figure S2c), and XRD (Figure S3) as detailed in the Supporting Information, in order to compare the electrocatalytic activity of the two selenides with the same morphology. The R_{ct} was 1.7 and 1.8 Ω cm^2 for particulate $Co_{0.85}Se$ and $Ni_{0.85}Se$, respectively, as estimated from Figure S4, suggesting that the two selenides with the same morphology had comparable electrocatalytic activity. As R_{ct} increased from the graphene-like (0.6 Ω cm^2) to particulate (1.7 Ω cm^2) morphology for the $Co_{0.85}Se$ sample, the graphene-like (or sheet) morphology should be favorable for high electrocatalytic activity.

It can be found that Z_N for the three symmetric cells also increases in the order of $Co_{0.85}Se$ (0.5 Ω cm^2) < Pt (0.9 Ω cm^2) < $Ni_{0.85}Se$ (1.4 Ω cm^2), which means that the diffusion coefficients (D) of triiodide for the cells vary in the inverse order, judged from eq 3, where k is the Boltzmann constant, T

$$Z_N = \frac{kT}{n^2 e_0^2 cA\sqrt{i\omega D}} \tanh\left(\sqrt{\frac{i\omega}{D}}\,\delta\right) \quad (3)$$

is the absolute temperature, n is the number of electrons involved in the electrochemical reduction of I_3^- at the electrode (here $n = 2$), e_0 is the elementary charge, c is the concentration of I_3^-, A is the electrode area, ω is the angular frequency, and δ is the thickness of the diffusion layer.[14] This result indicates that D increases with increasing electrocatalytic activity of the CE.

Figure 8 shows the Tafel polarization curves measured on the symmetrical cells used in EIS experiments. The slopes for the

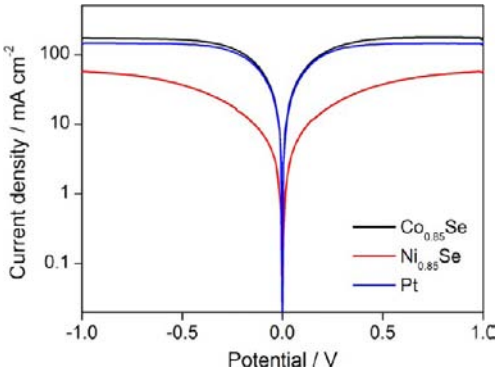

Figure 8. Tafel polarization curves of symmetrical cells fabricated with different CEs that are same as the ones used in EIS experiments.

anodic or cathodic branches are in the order of $Co_{0.85}Se$ > Pt > $Ni_{0.85}Se$. A larger slope in the anodic or cathodic branch indicates a higher exchange current density (J_0) on the electrode.[6a] J_0 can be also calculated by eq 4, where R_{ct} is the

$$J_0 = \frac{RT}{nFR_{ct}} \quad (4)$$

charge-transfer resistance obtained from EIS spectra (Figure 7), R is the gas constant, T is the absolute temperature, and F is Faraday's constant. Apparently, the calculated J_0 also follows the order of $Co_{0.85}Se$ > Pt > $Ni_{0.85}Se$, which is consistent with the J_{sc} order. In addition, the Tafel polarization curves contain the information about limiting current density (J_{lim}), which can be expressed by eq 5, where N_A is the Avogadro constant, l is the spacer thickness, and other parameters have been defined

dx.doi.org/10.1021/ja303034w | J. Am. Chem. Soc. 2012, 134, 10953−10958

$$J_{lim} = \frac{2ne_0DcN_A}{l} \quad (5)$$

previously.[14] As the value of J_{lim} increases in the order of $Co_{0.85}Se$ > Pt > $Ni_{0.85}Se$ and is directly proportional to the D, the latter should vary in the order of $Co_{0.85}Se$ > Pt > $Ni_{0.85}Se$, which is fairly consistent with the EIS analysis about the Z_N and D. Consequently, we conclude from the electrochemical and EIS results that graphene-like $Co_{0.85}Se$ has a higher electrocatalytic activity than Pt, and the latter is more active than particulate $Ni_{0.85}Se$. The order of electrocatalytic activity well explains the order of J_{sc}.

The electrochemical stability of the CEs was examined by repeated EIS measurements after aging or a pretreatment of CV scanning before each EIS measurement. Figure 9 shows the

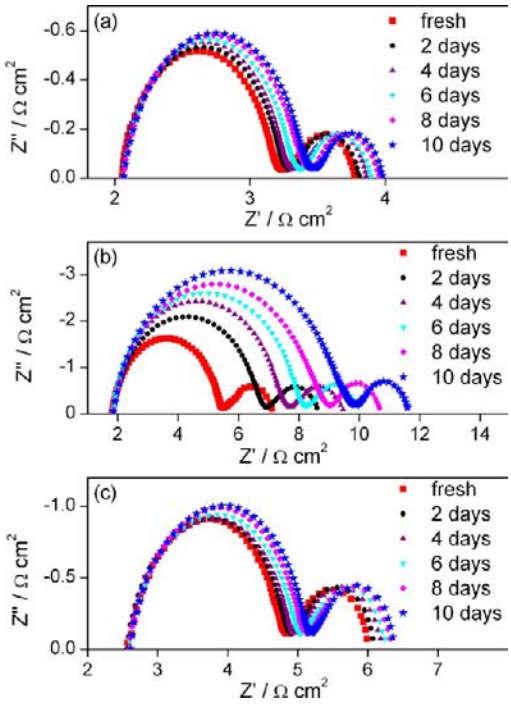

Figure 9. Nyquist plots of EIS for the symmetrical cells with $Co_{0.85}Se$ (a), $Ni_{0.85}Se$ (b), and Pt (c) electrode subjected to aging for some days at room temperature and open circuit.

impedance spectra for the fresh and aged dummy cells at room temperature and open circuit. For all the samples, R_s and Z_N hardly changed, indicating that the cell aging had almost no influence on the series ohmic resistance and the mass transport in the redox electrolyte solution. By contrast, the R_{ct} increased from 0.6 to 0.7 Ω cm^2 for $Co_{0.85}Se$, from 1.8 to 4.0 Ω cm^2 for $Ni_{0.85}Se$, and from 1.1 to 1.3 Ω cm^2 for Pt after aging for 10 days. This indicates that $Co_{0.85}Se$ and Pt had better electrochemical stability against aging than $Ni_{0.85}Se$.

Figure 10 shows the evolution of impedance spectra for the dummy cells subjected to sequential scans of CV and EIS for 10 cycles. After 10 cycles of scanning, there was negligible change in R_{ct} for $Co_{0.85}Se$ and Pt, while R_{ct} increased from 1.8 to 3.0 Ω cm^2 for $Ni_{0.85}Se$. This indicates that $Co_{0.85}Se$ and Pt had better electrochemical stability against potential cycling than $Ni_{0.85}Se$. For all the samples, there was almost no change of R_s and Z_N, meaning that the potential cycling hardly influenced the series

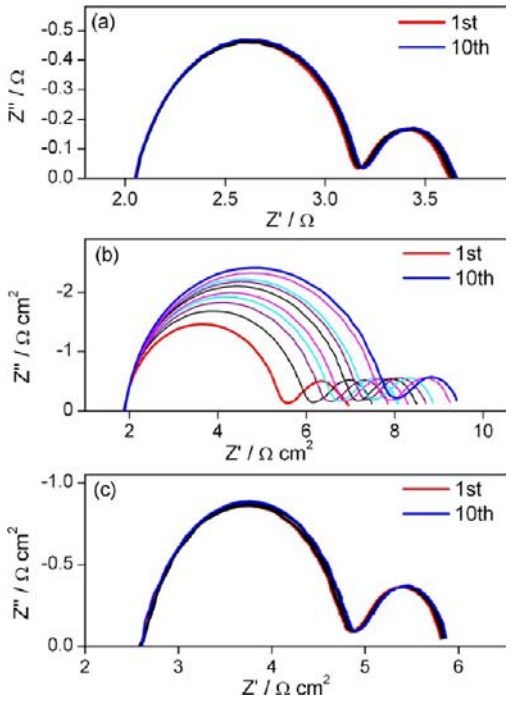

Figure 10. Nyquist plots of EIS for the symmetrical cells with $Co_{0.85}Se$ (a), $Ni_{0.85}Se$ (b), and Pt (c) electrodes. The cell was first subjected to CV scanning from 0 to 1 V and then from −1 to 0 V with a scan rate of 100 mV s^{-1}, followed by 20 s relaxation at 0 V, and then EIS measurement at 0 V from 0.1 Hz to 500 kHz was performed. This sequential electrochemical test was repeated 10 times.

ohmic resistance and the mass transport in the redox electrolyte solution.

The electrochemical stability of the particulate $Co_{0.85}Se$ against aging (Figure S5) and potential cycling (Figure S6) was also tested. Based on the stability data, the particulate $Co_{0.85}Se$ has an electrochemical stability comparable to that of particulate $Ni_{0.85}Se$ but poorer than that of graphene-like $Co_{0.85}Se$.

CONCLUSIONS

In summary, metal selenides, $Co_{0.85}Se$ and $Ni_{0.85}Se$, have successfully in situ grown on the surface of conductive glass through a facial one-step hydrothermal reaction at low temperature and shown to efficiently act as transparent counter electrodes in DSSCs without any post-treatments. $Co_{0.85}Se$ exhibits amazing electrocatalytic activity for the reduction of I_3^-, and the DSSC with it produces a higher short-circuit photocurrent and power conversion efficiency than the DSSC with a Pt CE. In consideration of this mild and facile approach, optical transparency, and low cost, selenide-based electrochemical catalysts have vast potential in scalable production of DSSCs. This finding paves the way for preparing cheap and highly efficient counter electrodes for DSSCs.

ASSOCIATED CONTENT

Supporting Information

EDS analysis of $Co_{0.85}Se$ and $Ni_{0.85}Se$ products obtained by hydrothermal reaction, HRTEM and FESEM images and XRD patterns for the particulate $Co_{0.85}Se$, comparison of the EIS for particulate $Co_{0.85}Se$ and $Ni_{0.85}Se$ electrodes, and electrochemical stability against aging or potential cycling of the

dx.doi.org/10.1021/ja303034w | J. Am. Chem. Soc. 2012, 134, 10953−10958

particulate $Co_{0.85}Se$ electrode. This material is available free of charge via the Internet at http://pubs.acs.org.

AUTHOR INFORMATION

Corresponding Author

zs.wang@fudan.edu.cn

Notes

The authors declare no competing financial interest.

ACKNOWLEDGMENTS

This work was financially supported the National Basic Research Program (2011CB933302) of China, the National Natural Science Foundation of China (20971025, 90922004, and 50903020), Shanghai Leading Academic Discipline Project (B108), and Jiangsu Major Program (BY2010147).

REFERENCES

(1) (a) O'Regan, B.; Grätzel, M. *Nature* **1991**, *353*, 737−740. (b) Grätzel, M. *Nature* **2001**, *414*, 338−344. (c) Yella, A.; Lee, H. W.; Tsao, H. N.; Yi, C.; Chandiran, A. K.; Nazeeruddin, M.; Diau, E. W.; Yeh, C. Y.; Zakeeruddin, S. M.; Grätzel, M. *Science* **2011**, *334*, 629−634.

(2) Xin, X.; He, M.; Han, W.; Jung, J.; Lin, Z. *Angew. Chem., Int. Ed.* **2011**, *50*, 11739−11742.

(3) (a) Lee, K. S.; Lee, W. J.; Park, N. G.; Kim, S. O.; Park, J. H. *Chem. Commun.* **2011**, *47*, 4264−4266. (b) Murakami, T. N.; Ito, S.; Wang, Q.; Nazeeruddin, M. K.; Bessho, T.; Cesar, I.; Liska, P.; Humphry-Baker, R.; Comte, P.; Péchy, P.; Grätzel, M. *J. Electrochem. Soc.* **2006**, *153*, A2255−A2261. (c) Han, J.; Kim, H.; Kim, D. Y.; Jo, S. M.; Jang, S. Y. *ACS Nano* **2010**, *4*, 3503−3509. (d) Kavan, L.; Yum, J. H.; Grätzel, M. *ACS Nano* **2011**, *5*, 165−172. (e) Kavan, L.; Yum, J. H.; Nazeeruddin, M. K.; Grätzel, M. *ACS Nano* **2011**, *5*, 9171−9178. (f) Kavan, L.; Yum, J. H.; Grätzel, M. *Nano Lett.* **2011**, *11*, 5501−5506. (g) Suzuki, K.; Yamaguchi, M.; Kumagai, M.; Yanagida, S. *Chem. Lett.* **2003**, *32*, 28−29.

(4) (a) Xia, J. B.; Masaki, N.; Jiang, K. J.; Yanagida, S. *J. Mater. Chem.* **2007**, *17*, 2845−2850. (b) Ahmad, S.; Yum, J. H.; Butt, H. J.; Nazeeruddin, M. K.; Grätzel, M. *ChemPhysChem* **2010**, *11*, 2814−2819. (c) Akhtar, S.; Kim, Y. S.; Yang, O. B.; Shin, H. S. *J. Phys. Chem. C* **2010**, *114*, 4760−4764.

(5) Gong, F.; Wang, H.; Wang, Z.-S. *Phys. Chem. Chem. Phys.* **2011**, *13*, 17676−17682.

(6) (a) Wang, M. K.; Anghel, A. M.; Marsan, B.; Ha, N. C.; Pootrakulchote, N.; Zakeeruddin, S. M.; Grätzel, M. *J. Am. Chem. Soc.* **2009**, *131*, 15976−15977. (b) Sun, H. C.; Qin, D.; Huang, S. Q.; Guo, X. Z.; Li, D. M.; Luo, Y. H.; Meng, Q. B. *Energy Environ. Sci.* **2011**, *4*, 2630−2637. (c) Wu, M. X.; Wang, Y. D.; Lin, X.; Yu, N. S.; Wang, L.; Wang, L. L.; Hagfeldt, A.; Ma, T. L. *Phys. Chem. Chem. Phys.* **2011**, *13*, 19298−19301.

(7) (a) Jiang, Q. W.; Li, G. R.; Gao, X. P. *Chem. Commun.* **2009**, *47*, 6720−6722. (b) Jiang, Q. W.; Li, G. R.; Liu, S.; Gao, X. P. *J. Phys. Chem. C* **2010**, *114*, 13397−133401. (c) Li, G. R.; Song, J.; Pan, G. L.; Gao, X. P. *Energy Environ. Sci.* **2011**, *4*, 1680−1683.

(8) (a) Wu, M. X.; Lin, X.; Hagfeldt, A.; Ma, T. L. *Angew. Chem., Int. Ed.* **2011**, *50*, 3520−3524. (b) Wu, M. X.; Lin, X.; Wang, Y. D.; Wang, L.; Guo, W.; Qi, D. D.; Peng, X. J.; Hagfeldt, A.; Grätzel, M.; Ma, T. L. *J. Am. Chem. Soc.* **2012**, *134*, 3419−3428.

(9) Norako, M. E.; Greaney, M. J.; Brutchey, R. L. *J. Am. Chem. Soc.* **2012**, *134*, 23−26.

(10) (a) Meng, Z.; Peng, Y.; Xu, L.; Yu, W.; Qian, Y. *Chem. Lett.* **2001**, *30*, 776−777. (b) Liu, X. H.; Zhang, N.; Yi, R.; Qiu, G. Z. *Mater. Sci. Eng. B-Solid* **2007**, *140*, 38−43.

(11) Wang, Z.-S.; Kawauchi, H.; Kashima, T.; Arakawa, H. *Coord. Chem. Rev.* **2004**, *248*, 1381−1389.

(12) Zhao, J.-F.; Song, J.-M.; Liu, C.-C.; Liu, B.-H.; Niu, H.-L.; Mao, C.-J.; Zhang, S.-Y.; Shen, Y.-H.; Zhang, Z.-P. *CrystEngComm* **2011**, *13*, 5681−5684.

(13) Roy-Mayhew, J. D.; Bozym, D. J.; Punckt, C.; Aksay, I. A. *ACS Nano* **2010**, *4*, 6203−6211.

(14) Hanch, A.; Georg, A. *Electrochim. Acta* **2001**, *46*, 3457−3466.